Crucial Role of Thermal Gradients in MMS Fluxgate In-Flight Calibration

Kenneth R Bromund[1], Bobby G Huang[2], Brian J Anderson[3], Guan Le[1], Mark Hubbert[4], Hanying Wei[4], Robert J Strangeway[4], Christopher T Russell[4], Rommel Zara[5] and Santino Rosanova[5], Ferdinand Plaschke[6], David Fischer[7] and Werner Magnes[7]

(1) NASA Goddard Space Flight Center, Greenbelt, MD, United States
(2) ADNET/NASA GSFC, Greenbelt, United States
(3) Johns Hopkins Univ, Laurel, MD, United States
(4) University of California Los Angeles, Los Angeles, CA, United States
(5) Vertex Aerospace LLC / NASA GSFC, Greenbelt, United States
(6) IWF ÖAW, Graz, Austria
(7) Austrian Academy of Sciences, Space Research Institute, Graz, Austria

For more information, contact kenneth.r.bromund@nasa.gov

SH35D-2103

Overview

Magnetic field measurements are critical to the success of the Magnetospheric Multiscale (MMS) mission. To meet the science goals of the mission, the Fluxgate Magnetometer (FGM) instrument must measure the ambient magnetic field with an accuracy of 0.1 nT. The in-flight calibration process uses the spacecraft spin to determine the offset (or zero level) of the sensor at ~15 minute time scale, revealing that on a typical MMS orbit, the offsets (or zero levels) of the 3-axis FGM can vary by ~0.5 nT (exclusive of periods in Earth shadow). The variations in the ambient field within the MMS region of interest (ROI) limit the precision of these dynamic measurements. Thus, empirically determined relationships of the offset vs sensor temperature are used to determine the offset within the ROI. However, this approach raises new questions and has some limitations:

1) Why do offsets respond to sensor temperature differently in sunlight vs. shadow?
2) Why does the offset baseline change abruptly after maneuvers?
3) Why do offsets deviate from the sensor temperature relationship near perigee?

We address these questions by considering the the fact that thermal load from the Sun and the Earth will change as a function of spacecraft attitude and position.

Background

The MMS FGM Instrument

MMS consists of 4 spacecraft (MMS1, MMS2, MMS3 and MMS4) flying in close (10-100 km) formation. Each is equipped with an FGM instrument comprised of two 3-axis fluxgate magnetometers, AFG and DFG, mounted on opposite booms (Fig. 1 at right).

AFG and DFG provide redundancy and complement one another. The two independent measurements compared and combined to provide the most accurate measurement.

AFG and DFG share the same sensor design (Fig. 2 below), but have distinct and independent electronics mounted on the spacecraft deck.

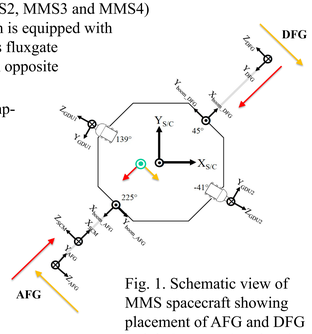

Fig. 1. Schematic view of MMS spacecraft showing placement of AFG and DFG and their respective chassis coordinate systems relative to spacecraft (S/C) coordinates, as well as the nominal orientations of the sensor 1,2,3 axes used for in-flight calibration. Red and Yellow arrows indicate the direction of the external magnetic field that would be required near each sensor to produce the additional offsets associated with increased spacecraft tilt towards the sun.

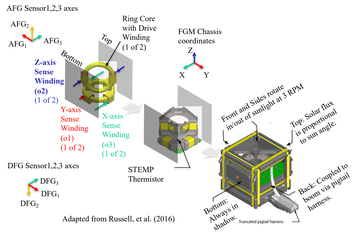

Fig. 2. FGM sensor assembly breakdown
(a) Sense and drive windings,
(b) Armatures and PC board with thermistor,
(c) Assembeled chassis with feedback windings and harness.

In-Flight Orthogonalization

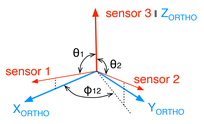

Fig. 3.

On a spin-stabilized spacecraft, 8 parameters can be determined on 15-30 minute intervals by minimizing spin tone and second harmonic signals [Anderson, et al., 2022]

In addition to the orthogonality angles θ_1, θ_2, and φ_{12} shown Fig 3, and the projection of the sensor 3 axis onto the spin plane, s_x, s_y, shown in Fig 4, orthogonalization determines relative gain of sensor 1 and 2, dg_{sp}, and the offsets on sensor 1 and 2, o_1 and o_2, respectively.

Mystery #1: Different Behavior In Sunlight and Shadow

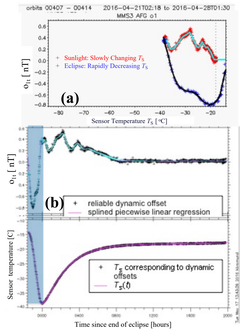

Fig. 5 An ensemble of 7 orbits showing the dynamic offsets, o1, measured on 15-min intervals for MMS3 AFG sensor 1. (a) o1 plotted with respect to sensor temperature, T_S, with spline fits shown for times in sunlight (cyan) and eclipse (black). Superposed epoch of measurements of o1 (b) and T_S (c), referenced to the time of minimum T_S on each orbit. In (b) the offset fits to temperature shown in (a) are mapped to into the time domain (cyan), showing excellent agreement with measured o1 (black +). Shaded region indicates eclipse.

In the low field regime of the MMS region of interest (ROI), offsets are the primary source of measurement error, and must be characterized accurately.

MMS offsets are corrected using a technique that characterizes the relationship of offset to sensor temperature, T_S, enabling offsets to be corrected to <0.200 nT [Anderson, et al, 2022].

A baseline offset, o_{ib}, is determined on each sensor, *i*, for the sunlit portion of each orbit. The residual o_R is fit to two separate spline functions of sensor temperature on 7-day intervals:

$o_R{}^S(T_S)$ for times in sunlight, and

$o_R{}^E(T_S)$ for times in eclipse

Mystery #2: Offset Baseline Jumps at Maneuvers

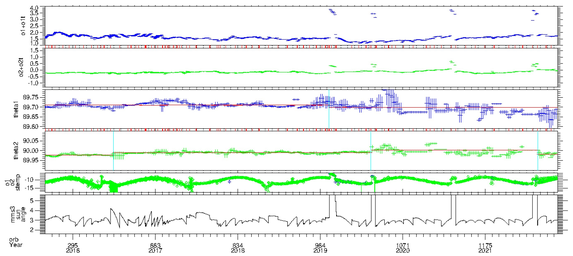

Fig. 6. Mission Trend of orthogonalization parameters for MMS3 DFG: median values of o_1 and o_2 for each orbit. Also shown are sensor temperature, T_S, and Sun Angle, δ. Times of maneuvers are indicated by vertical bars in red between each of the panels

The apparent correlation between the offset changes at maneuvers and the Sun Angle changes suggests a linear relationship. See Fig 10!

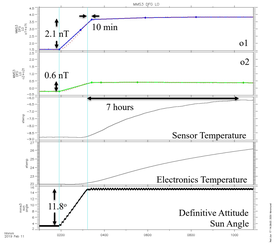

Fig 7: Evolution of offsets, temperatures, and sun angle during tilt maneuver.

10 minute delay in response of offsets to sun angle, vs 7 hour delay for sensor temperature

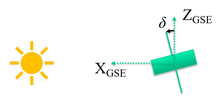

Could it be... the Sun?

Mystery #3: 'Hockey Sticks' Near Perigee

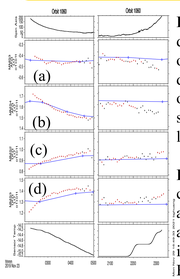

Fig. 8. For ascending (left) and descending (right) portion of the orbit: Spin axis field (top); dynamic offsets and expected offset from T_S trend for selected sensors (a,b,c,d) that exhibit the largest residuals; T_S (bottom).

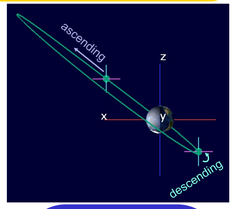

Fig 9. MMS orbit in GSE coordinates, showing attitude and position of MMS in the ascending and descending intervals shown in Fig. 8. Each axis extends to 4 R_E.

Could it be... the Earth?

Some sensors show 'hockey sticks': e.g. in Fig 8 panel (b), o1 decreases with proximity to the Earth even though T_S is constant, and then begins high after perigee and decreases with distance from perigee in a way that cannot be modeled as a function of T_S (in Fig 14a, note the red points at the highest temperatures). Residuals can be as large as 0.2 nT at 4-5 Earth radii (R_E). Note that the direction of the 'hockey stick' deviations alternates ascending vs descending. Similarly, Earth's Outgoing Longwave Radiation (OLR) will shine onto the bottom of the spacecraft while ascending, and onto the top while descending (Fig 9).

A Clue: Correspondence Between Earth and Sun Effects

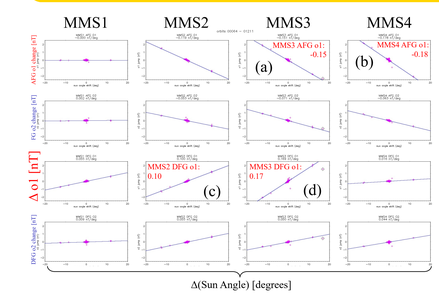

Fig 10. Linear fits to observed change in offset at each maneuver vs change in sun angle, δ, for each spin-plane sensor. The sensors labeled (a), (b), (c) and (d) are the sensors indicated in Fig. 8.

Note the correspondence in sign and magnitude of the hockey stick effects in Fig 8 and the sign and magnitude of the sun angle dependences shown here.

The Smoking Gun: Thermal Modeling Results

Thermal load from Sunlight on top face will create a thermal gradient along the spin axis proportional to $\sin(\delta) = \hat{\mathbf{r}}_S \cdot \hat{\mathbf{L}}$

This thermal load disappears during eclipse, and thermal models of the FGM sensor (Fig 12) show that thermal gradients drop to zero with an e-folding time of ~30 minutes, while T_S response time is > 5 hrs. This corresponds to the observations in Fig. 5.

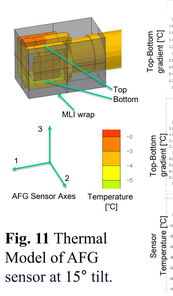

Fig. 11 Thermal Model of AFG sensor at 15° tilt.

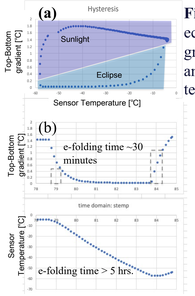

Fig 12: Thermal Model Results for an eclipse at 15° tilt: Hysteresis of thermal gradients with respect to temperature **(a)** and time evolution of gradients and temperature **(b)**.

Fig 13: Thermal Model results for an orbit like that in Fig 9: Gradients and temperature near perigee

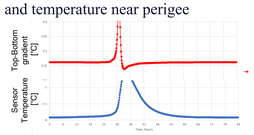

Application: De-coupling Thermal Gradient from Temperature

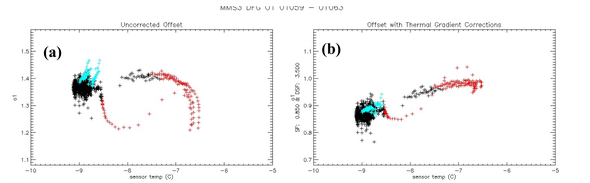

Fig 14. Offset vs Temperature (a) before and (b) after correction for thermal loading effects

A simple model corrects for the changing thermal load:

$$S_i(\hat{\mathbf{r}}_S \cdot \hat{\mathbf{L}}) + \frac{S_i \cdot C \cdot D \cdot (\hat{\mathbf{r}}_E \cdot \hat{\mathbf{L}})}{4(r_E/R_E)^2}$$

S_i is the linear factor determined for each sensor as a response to small angles of sunlight (Fig. 10). *C* is an empirically determined constant of proportionality that accounts for differences emissivity of insulation to full spectrum sunlight vs IR, and for the intensity of IR from Earth, as compared to the energy flux from the sun. The unit vectors *to* the Sun and Earth are $\hat{r}_S$ and $\hat{r}_E$, respectively.

The same factor *C* works for all sensors and is well constrained, because measurements are available both as temperatures decrease outbound at larger r_E when unaffected by Earth's thermal load (black in Fig 14) and inbound, when temperatures again increase (cyan) .

We find that the –Z face appears to be more sensitive to OLR than the +Z face by an empirically determined factor, *D*, which is applied when OLR illuminates the –Z face (red). In general, *D* is poorly constrained, and factors in the range 3-10 can all achieve acceptable results. In this example, a lunar eclipse right after perigee lowers the temperature during the time when the thermal load changes, showing that a factor of 3.5 may be best.

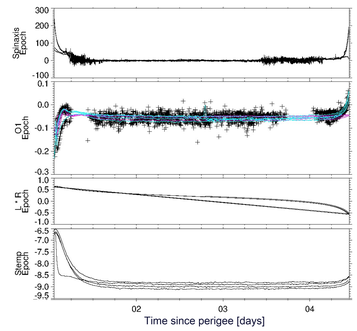

Fig 15. Superposed epoch of 4 orbits (2019-11-19 - 2019-12-03) for MMS3 DFG. Top to bottom: measurement of B along spin axis; o1 with fit to T_S alone (cyan) and fit after accounting for thermal load (magenta); $\hat{\mathbf{r}}_E \cdot \hat{\mathbf{L}}$; and sensor temperature. T_S

Discussion

The thermal gradient errors cannot be attributed to a dipole field from the spacecraft. See Fig. 1 for an illustration of the fields required to explain the results summarized in Fig. 10. The field must be generated near the sensor and may be an inherent property of the fluxgate itself. For example, it maybe be due to diamagnetic currents within the ring core.

We note that the changing offsets have implications for the determinations of the angular parameters θ_1, θ_2 and φ_{12} (c.f. Fig. 3), discussed in detail in Bromund, et al. [2022]. However, these effects are on the order of 0.02° and do not impact mission accuracy goal, except rare cases when the ROI extends to low altitudes.

To meet MMS goals, the simple model presented here is sufficient. It requires only definitive attitude and ephemeris as input, and thus no on-board measurement of the gradient is necessary. There are mission scenarios in which it would be essential to measure the thermal gradients as well as the temperature within the sensor.

References

Bromund, et al. [2022, in preparation], Critical Role of Thermal Gradients in MMS Fluxgate In-Flight Calibration

Anderson, B. J. et al. [2022, in preparation], In-Flight Calibration and Performance of the Magnetospheric Multiscale Fluxgate Magnetometers, Space Sci. Rev.

Russell, et al. (2014). The Magnetospheric Multiscale Magnetometers. Space Sci Rev.; DOI: 10.1007/s11214-014-0057-3